Supporting Information

Reactive Lithium Fluoride Revitalizes Bulk-interface Na-ion Transport in All-solid-state PEO-based Sodium Batteries

You Fan[#], Binghong Zhao[#], Xin Zou, Wenlong Zhao, Yanyan Zhang, Meizhen Zhu, Hong Zhang, Zige Hong, Xin Cheng, Peiming Chen, Zhengshuai Bai*, Yanbin Shen, Yuxin Tang**

Dr. Y. Fan, B. Zhao, X. Zou, W. Zhao, M. Zhu, H. Zhang, Z. Hong, X. Cheng, P. Chen, Prof. Y. Tang
College of Chemical Engineering, Fuzhou University, Fuzhou 350116, P. R. China
E-mail: zyanyan@fzu.edu.cn; baisz@fzu.edu.cn

Dr. H. Zhang, Prof. Y. Tang
Qingyuan Innovation Laboratory, Quanzhou 362801, China
E-mail: yxtang@fzu.edu.cn

W. Zhao, Y. Shen
i-Lab, Suzhou Institute of Nano-tech and Nano-Bionics, Chinese Academy of Sciences, Suzhou 215123, China

# Y. Fan and B. Zhao contributed equally to this work.

Funding:
National Key R & D Program of China (2024YFE0101600)
National Natural Science Foundation of China (22279017)
Platform Supporting Fund of Qingyuan Innovation Laboratory (Grant No. 00623001)
Startup Fund of Qingyuan Innovation Laboratory (Grant No. 00524009)
Key Program of Qingyuan Innovation Laboratory (Grant No. 00223002)

Experimental Section

Materials. Commercially available chemicals of poly(ethylene oxide) (PEO, M_W = 600,000 g mol^{-1}, Sigma-Aldrich), Sodium Trifluoromethanesulfonate (NaOTf, 98%, Macklin), LiF (purity 99.99%, Macklin), NaF (purity 99.99%, Macklin) were dried before use.

Fabrication of PEO–based polymer electrolyte.

The PEO–based polymer electrolyte was prepared by a solution casting technique using anhydrous acetonitrile (ACN) as the solvent. Initially, PEO and NaOTf (EO: Na = 20:1) were thoroughly dissolved in acetonitrile under continuous stirring, a mixture of different fluorides was added to the above solution. The weight ratio of fluorides was fixed at 5 wt%. The resulting gelatinous solution was stirred for 12 h, and then poured onto a polytetrafluoroethylene (PTFE) mold, followed by drying under vacuum for 16 h.

Once fully dried, the PEO-based solid polymer electrolyte membrane was gently removed from the PTFE mold and hot pressed at 70°C for 3 minutes with a holding pressure of 10 MPa, resulting in a 70±5 μm electrolyte membrane that was punched into a round shape with a diameter of 16.5 mm. All procedures were performed in a drying room with a relative humidity of less than 5% and a dew point temperature lower than -40°C. These as-prepared electrolyte membranes were immediately transferred to the glove box for further use.

Preparation of cathodes and assemble of batteries.

The $Na_3V_2(PO_4)_3$ (NVP) cathode slurry was formulated with 70% NVP, 10% Ketjen black, and 20% PEO. It was then blade-coated onto Al foils and dried at 80°C for 12 hours. The resulting cathode plate was punched into round pieces of φ12mm with a loading of 3.0±0.1 mg cm^{-2} and stored in an Ar-filled glove box for subsequent cell assembly. Before charge/discharge or electrochemical tests, all CR2032 coin cells were heated at 65 °C for 24 hours.

Characterization.

X–ray Diffraction results of the polymers were determined by an X–ray diffractometer (D/MAX-Ultima-X) with a scanning speed of 8°/min from 5 to 80°. For Fourier transform infrared (FTIR) transmittance spectroscopy, polymer electrolytes were pressed on the FTIR instrument (AVATAR360). FTIR data were collected at room temperature from 400 to 4000 cm^{-1} (4 cm^{-1} resolution). Differential scanning calorimetry (DSC, DSC214) was performed by Diamond DSC at 5 ℃ min from -100 to 100 ℃ under N_2 atmosphere. The crystallinity (χ_c) can be calculated by the Equation (1):

$$\chi_c = \frac{\Delta H_f}{\Delta H_f^o} \tag{1}$$

where ΔH_f^o (133.65 J g^{-1}) is the melting enthalpy of a completely crystalline PEO sample and is the experimental enthalpy. The morphologies of samples were examined by field emission scanning electron microscope (Nova NanoSEM 230) equipped with Energy Dispersive X-ray Spectroscopy (EDS). Solid-state ^{1}H and ^{23}Na magic-angle spinning (MAS) nuclear magnetic resonance (NMR) spectra were collected by Bruker avance III 500 MHz NMR spectrometer. Raman spectroscopy data were recorded from 100 to 4000 cm^{-1}. X-ray photoelectron (XPS, ESCALAB 250) measurements were carried out to analyze the surface chemical environment of PEO-based polymer electrolytes and sodium anodes after cycling. Time-of-flight secondary ion mass spectrometry (TOF-SIMS) analysis was performed using a TOF-SIMS 5 spectrometer (ION-TOF GmbH). Elemental depth profiles were acquired using Bi^+ ions for analysis at 10 kV and Cs^+ ions for sputtering at 2 kV and 20 nA. The charge/discharge performance of NVP-based ASS cells was evaluated with the Neware battery test system under various current densities. The mechanical properties of the electrolyte membranes were evaluated by using a universal testing machine (EZ TEST, Shimadzu, Japan). For the tensile tests, an elongation speed of 20 $mm \cdot min^{-1}$ at 25.0 ℃ and a relative humidity of 30.0%. For the puncture tests, a 1 mm-thick needle with a spherical tip was used to puncture the polymer electrolyte membrane at a puncture rate of 5

mm/min until the membrane was completely punctured by the needle. Before measurements, the membranes were cut into standard samples with dimensions of 20 mm*6 mm*60 μm. Renishaw Invia Reflex was utilized to record the Raman absorbance of as-prepared electrolyte membranes.

Electrochemical measurements

The polymer PEO electrolyte membranes were cut into plates with a diameter of 16.5 mm. Symmetric Na/Na cells were assembled by placing two sodium plates with a diameter of 16.5 mm on both sides of the membrane. The sandwich-like units were sealed in a 2032 coin cell. Ionic conductivities of SPEs were tested by electrochemical impedance spectroscopy (EIS). The operation temperature is from 35 to 85 ℃ and the test frequency is from 1 MHz to 1 Hz. The ionic conductivity (σ) was calculated based on the Equation (2):

$$\sigma = \frac{L}{RS} \tag{2}$$

where the L is the thickness of the electrolyte membrane, R is the resistance of the cell obtained from the EIS spectrum, S is the area of the sodium plate. The sodium-ion transference number (t_{Li^+}) was obtained from the symmetric Na/Na cell at 65 °C based on the Equation (3):

$$t_{Li^+} = \frac{I_s(\Delta V - I_0 R_0)}{I_0(\Delta V - I_S R_S)} \tag{3}$$

where the ΔV is the polarization voltage, I_0 and R_0 are the current and resistance of the initial state, and the I_s and R_s are the current and resistance of the stable state, respectively. All the electrochemical data were collected by a CHI600E electrochemical workstation.

Theoretical calculations.

The simulations were performed using COMSOL Multiphysics to analyze the impact of different electrolytes on the distribution of ion concentration and over potential

during the deposition process. In general, the models are constructed based on interfaces of “Tertiary Current Distribution” and “Level Set”. The concentration and over potential in were analyzed using the “Tertiary Current Distribution” module[s1]. Meanwhile, the growth of Na dendrite was simulated by coupling “Level Set” module[s2]. The ion concentration followed Fick's First Law for diffusion, while electro-migration followed the Nernst-Planck relationship, and the reaction on the electrode surface followed the Butler-Volmer equation. The surfaces of the electrode were operated under the exchange current density of 10 A m^{-2}. The simulations provided steady-state solutions for concentration trends over time. The total deposition time is 300 s, and the geometric dimensions of the model are 10 μm*12 μm.

According to Nernst-Einstein Equation (4):

$$\sigma = nqD\frac{q}{K_B T} \tag{4}$$

where σ represents the ionic conductivity of the electrolyte, n represents the concentration of the mobile charge carriers (ions), q represents the charge carried by each ion, D represents the diffusion coefficient, K_B represnets the Boltzmann constant, and T represents the absolute temperature.

The explanation of the application of Thompson-Gibbs equation in this study[s3, s4]

The Thompson-Gibbs equation plays a critical role in understanding polymer crystallization by relating crystal size to thermodynamic properties. The equation corrects for curvature effects in small crystals, linking observed melting temperature (T_m) to the equilibrium melting point (T_m^0), which can be expressed as Equation (5):

$$T_m = T_m^0 - \frac{2\sigma_e T_m^0}{\Delta H_f l} \tag{5}$$

where σ_e represents the surface free energy of folded chains, ΔH_f represents the heat of fusion, and l represents the thickness of crystal layers.

In this study, Thompson-Gibbs equation is utilized to correlate the polymer melting point with the size (completeness) of the crystalline region. Through this, the

influence of reactive fluorides on the orientation and arrangement of polymer chain segments through the formation of intermolecular interactions was investigated.

Discussion of the crystalliny of electrolytes in this study

Our supplemented quantitative DSC results confirm these correlations: For P-PEO (pristine electrolyte), the melting peak is centered at ~64.0 °C (dominated by well-ordered crystalline regions) with a narrow FWHM of 3.2 °C and ΔH_f of 50.9 J g^{-1}, corresponding to a χ_c of ~38.2%—indicating large, defect-free crystalline domains and a small amorphous fraction. For L-PEO (5 wt% LiF), the melting peak shifts down to ~61.5 °C (due to abundant incomplete crystalline regions) with a broadened FWHM of 4.5 °C and reduced ΔH_f of 36.7 J g^{-1}, resulting in a χ_c of ~27.5%—the broader FWHM quantifies the smaller size and lower integrity of PEO crystalline domains, while the reduced χ_c directly confirms an expanded amorphous region (from ~61.8% in P-PEO to ~72.5% in L-PEO). For S-PEO (5 wt% NaF, control), the FWHM is 3.8 °C, ΔH_f is 43.0 J g^{-1}, and χ_c is ~32.1%—values between P-PEO and L-PEO—consistent with NaF's weaker ability to induce incomplete crystalline regions compared to LiF. These quantitative data collectively validate that LiF-mediated supramolecular interactions promote the formation of incomplete crystalline regions (quantified by broader FWHM), reduce overall crystallinity (quantified by lower ΔH_f and χ_c), and expand the amorphous fraction—all of which facilitate Na^+ transport.

Supporting Figures

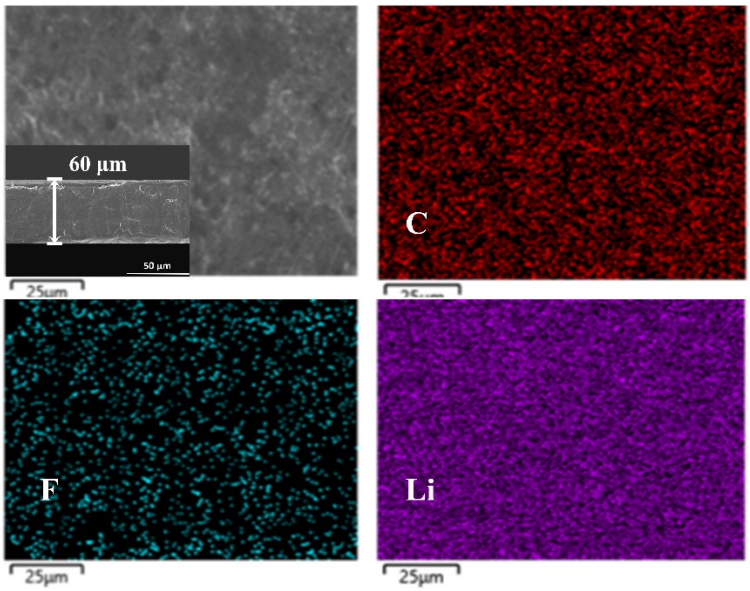

Fig. S1 The morphology and EDS-mapping of L-PEO.

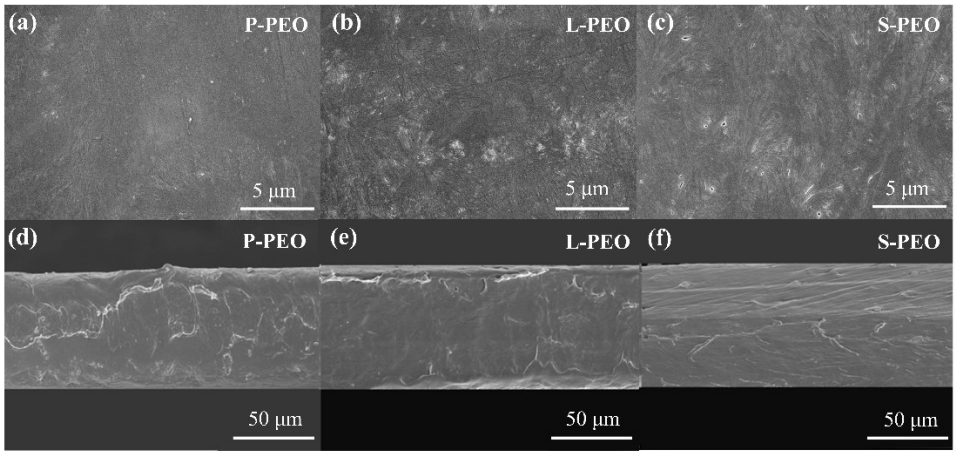

Fig. S2 The SEM planar and cross-sectional image of P-PEO, L-PEO and S-PEO.

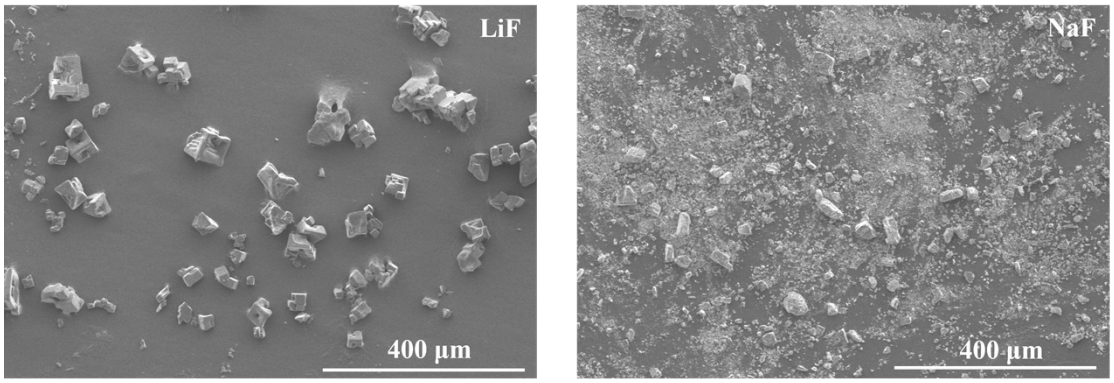

Fig. S3 The SEM of LiF and NaF.

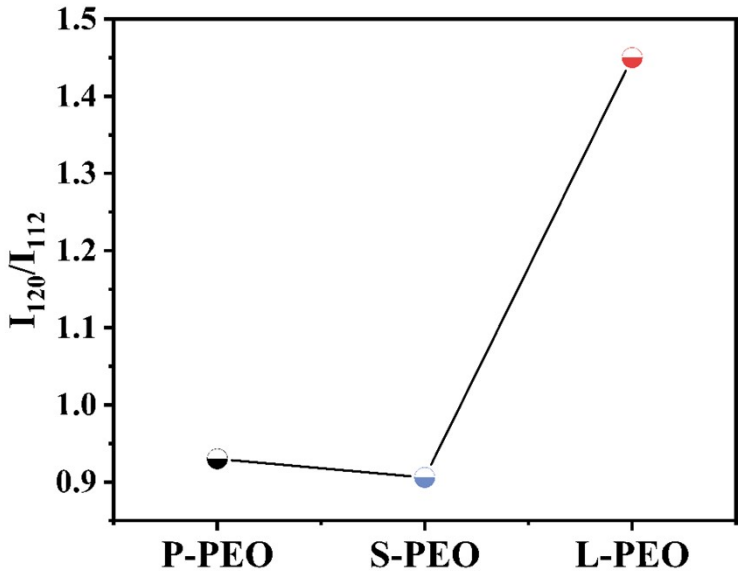

Fig. S4 The I_{120}/I_{112} of XRD signals of P-PEO, L-PEO and S-PEO.

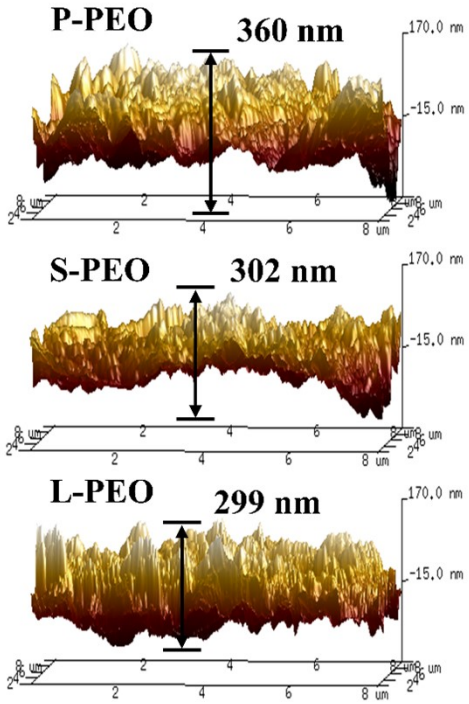

Fig. S5 The AFM 3D image of P-PEO, L-PEO and S-PEO.

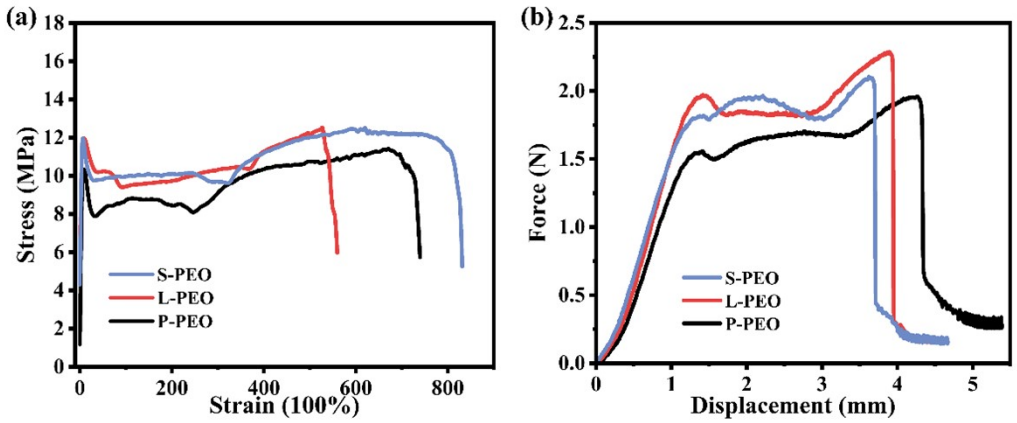

Fig. S6 The (a) tensile and (b) puncture mechanical properties of P-PEO, L-PEO and S-PEO.

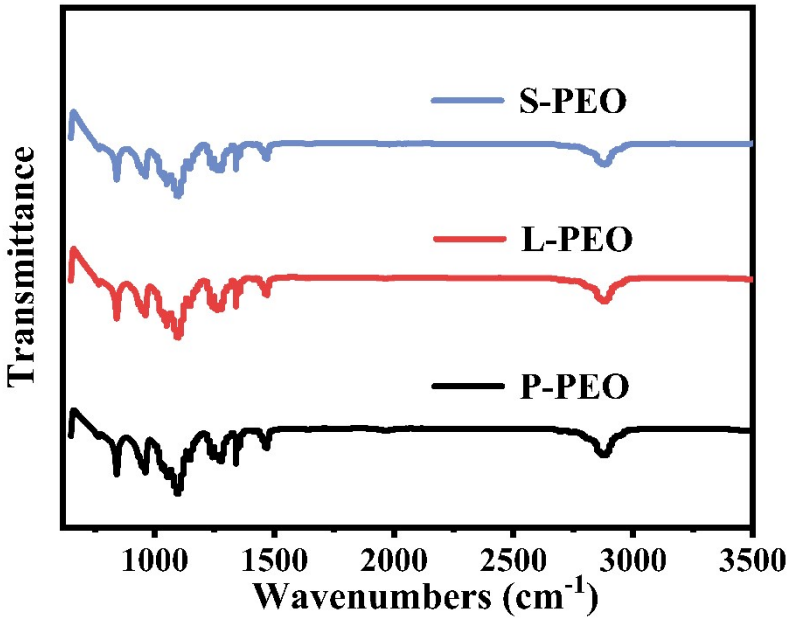

Fig. S7 The FTIR of P-PEO, L-PEO and S-PEO.

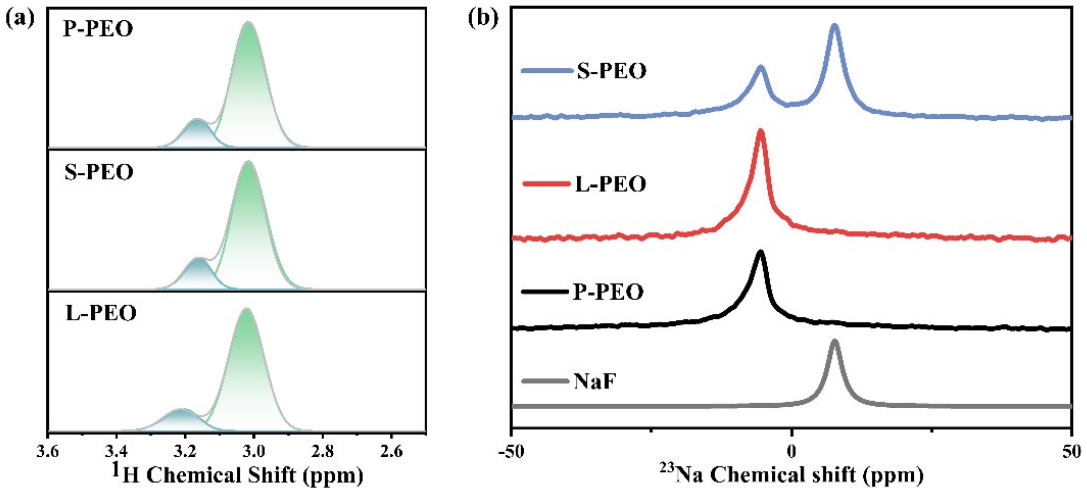

Fig. S8 The (a)^{1}H and (b)^{23}Na solid-state NMR spectra of P-PEO, L-PEO and S-PEO.

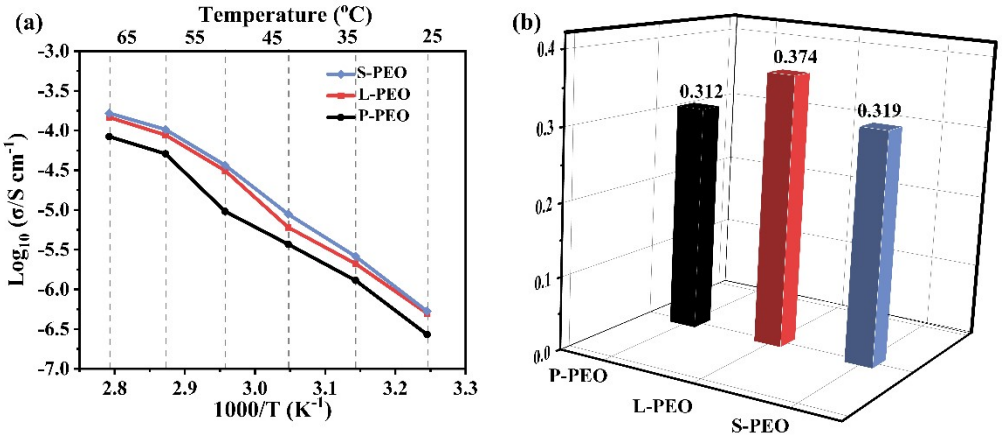

Fig. S9 The (a)Arrhenius diagrams and (b)Li^{+} transference number at 65 °C of P-PEO, L-PEO and S-PEO.

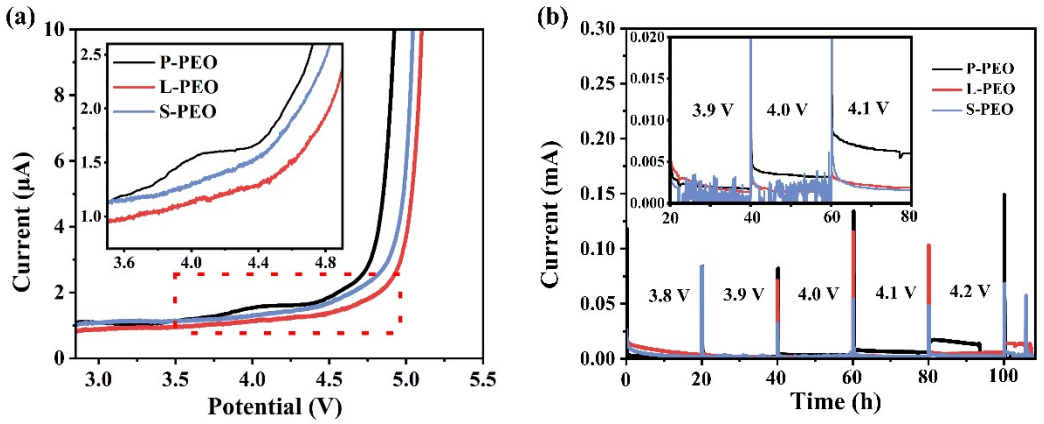

Fig. S10 The (a)linear sweep voltammetry plots and (b)Electrochemical floating analysis using NVP cathodes of P-PEO, L-PEO and S-PEO.

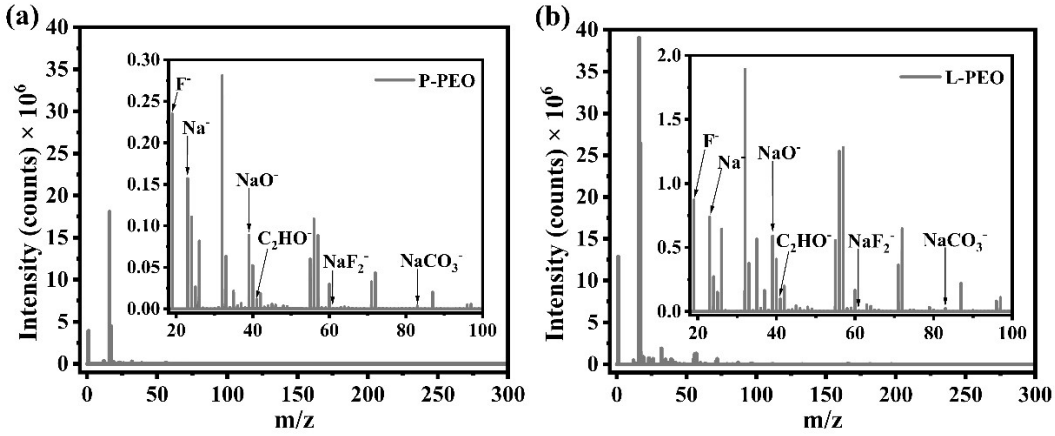

Fi

g. S11 TOF-SIMS mass spectrum of (a)P-PEO and (b)L-PEO.

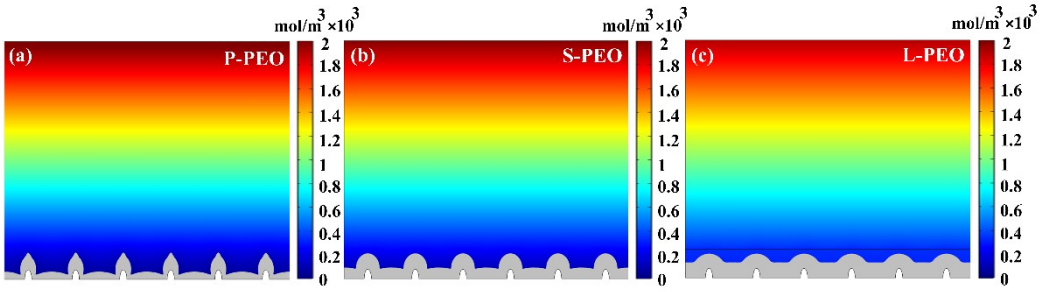

Fig. S12 FEA Simulated concentration distribution of solid-state Na battery system with (a) P-PEO, (b) S-PEO and (c) L-PEO.

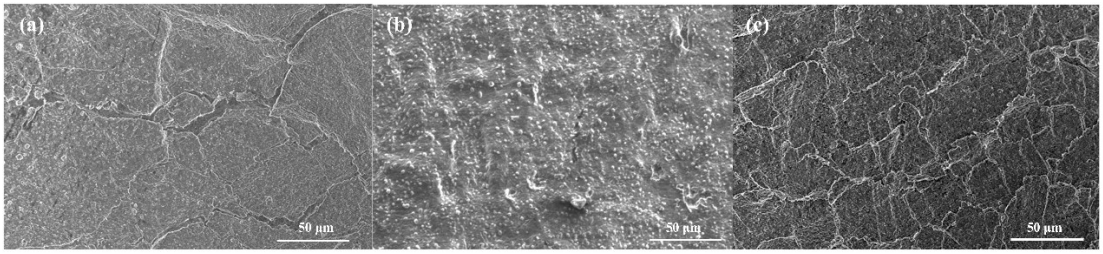

Fig. S13 SEM images of Na after cycling in (a) Na|P-PEO|NVP, (b) Na|S-PEO|NVP, and (c) Na|L-PEO|NVP cells (Na stripping).

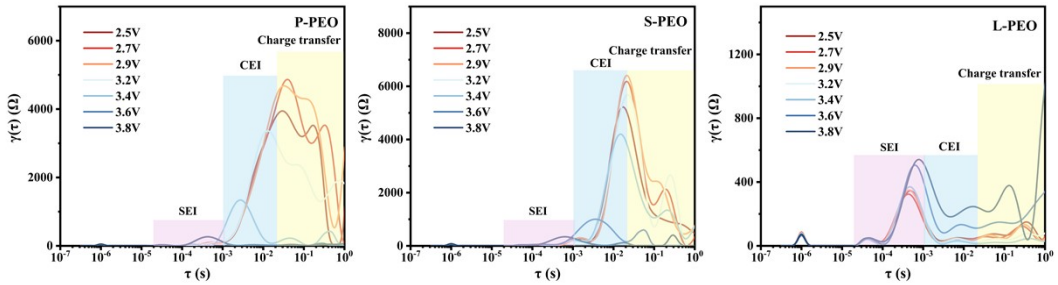

Fig. S14 DRT analysis of NVP||Na cells with (a) P-PEO, (b) S-PEO, and (c) L-PEO at different charging voltages.

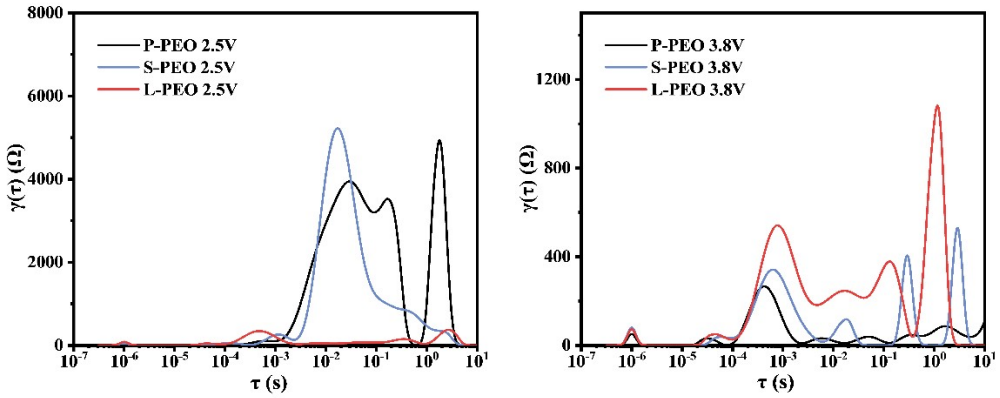

Fig. S15 DRT analysis of NVP||Na batteries with P-PEO, S-PEO, and L-PEO under 2.5V (left) and 3.8V (right) charging voltages.

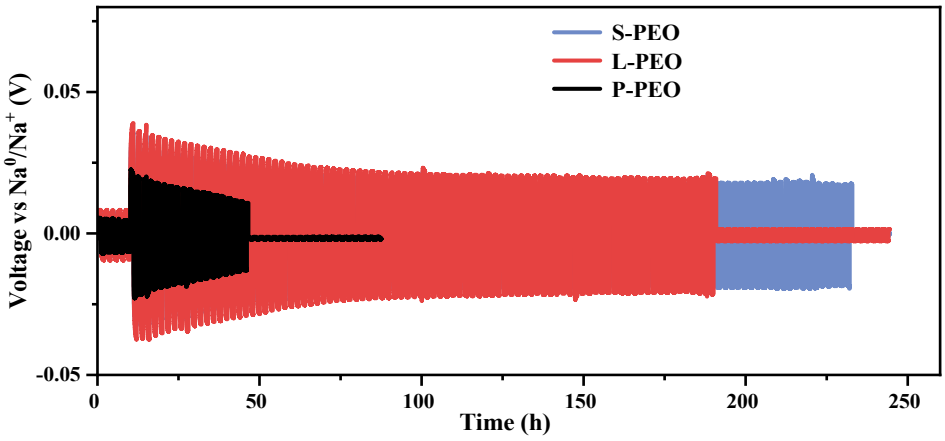

Fig. S16 Cycling performance (with a fixed current density and capacity of 0.1 mAh cm^{-2} and 0.1 mA cm^{-2}) of Na||Na symmetrical cells with P-PEO, L-PEO and S-PEO.

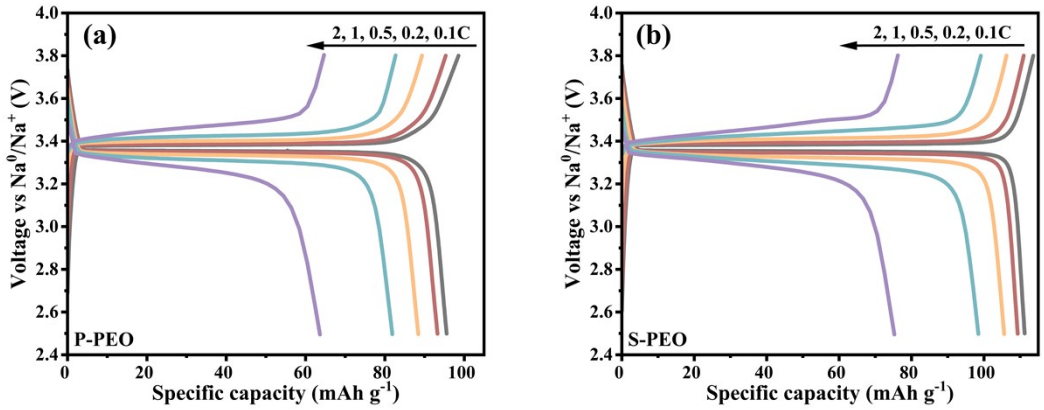

Fig. S17 Voltage profiles of NVP||Na cells with (a) P-PEO and (b) S-PEO.

Table S1: The diffusion coefficients of SPEs.

SPEs	Cation	Anion
P-PEO	4×10^{-14} m^{-2} s^{-1}	8.8×10^{-14} m^{-2} s^{-1}
S-PEO	1.58×10^{-13} m^{-2} s^{-1}	3.36×10^{-13} m^{-2} s^{-1}
L-PEO	1.55×10^{-13} m^{-2} s^{-1}	2.59×10^{-13} m^{-2} s^{-1}

Table S2: Spectroscopic Peak Assignments (740.0~780.0 cm^{-1}).

Raman/IR freq.(cm^{-1})	Assignment
753	Free anions
763	Compound I
770	Compound II

Table S3: Spectroscopic Peak Assignments (1000.0~1100.0 cm^{-1}).

Raman freq.(cm^{-1})	IR freq.(cm^{-1})	Assignment
-	1025	Other compound
1031	1032	Free anions
1037	1037	Ion pairs
1048	1050	Compound I
1060	~1057	Compound II

References

[s1] Z. Xu, L. Xu, Z. Xu, Z. Deng and X. Wang, *Adv. Funct. Mater.*, 2021, **31**, 2102354.

[s2] T. Zeng, Y. Yan, M. He, D. Du, X. Wen, B. Zhou and C. Shu, *J. Mater. Chem. A*, 2022, **10**, 23712–23721.

[s3] A. Toda, *Polym. J.*, 2025, **57**, 1049–1065.

[s4] K. Iwata, *Polymer*, 2002, **43**, 6609–6626.